Geophysical Journal International

Geophys. J. Int. (2013) doi: 10.1093/gji/ggt146

Gravity effect of water storage changes in a weathered hard-rock aquifer in West Africa: results from joint absolute gravity, hydrological monitoring and geophysical prospection

Basile Hector,[1] Luc Séguis,[2] Jacques Hinderer,[1] Marc Descloitres,[3] Jean-Michel Vouillamoz,[3] Maxime Wubda,[3] Jean-Paul Boy,[1] Bernard Luck[1] and Nicolas Le Moigne[4]

[1] *IPGS-EOST, CNRS/UdS, UMR 7516, 5 rue René Descartes, 67084 Strasbourg Cedex, France. E-mail: basile.hector@unistra.fr*
[2] *IRD/CNRS/UM2/UM1, UMR HydroSciences Montpellier, Place E. Bataillon, F-34095 Montpellier Cedex 5, France*
[3] *IRD/UJF-Grenoble-1/CNRS/G-INP – UMR LTHE, 08 BP 841 Cotonou, Benin*
[4] *Géosciences Montpellier, UMR CNRS/UM2 5243, Montpellier, France*

Accepted 2013 April 9. Received 2013 April 8; in original form 2012 August 19

SUMMARY

Advances in groundwater storage monitoring are crucial for water resource management and hydrological processes understanding. The evaluation of water storage changes (WSC) often involve point measurements (observation wells, moisture probes, etc.), which may be inappropriate in heterogeneous media. Over the past few years, there has been an increasing interest in the use of gravimetry for hydrological studies. In the framework of the GHYRAF (Gravity and Hydrology in Africa) project, 3 yr of repeated absolute gravity measurements using a FG5-type gravimeter have been undertaken at Nalohou, a Sudanian site in northern Benin. Hydrological data are collected within the long-term observing system AMMA-Catch. Once corrected for solid earth tides, ocean loading, air pressure effects, polar motion contribution and non-local hydrology, seasonal gravity variations reach up to 11 μGal, equivalent to a WSC of 260-mm thick infinite layer of water. Absolute temporal gravity data are compared to WSC deduced from neutron probe and water-table variations through a direct modelling approach. First, we use neutronic measurements available for the whole vertical profile where WSC occur (the vadose zone and a shallow unconfined aquifer). The RMSD between observed and modelled gravity variations is 1.61 μGal, which falls within the error bars of the absolute gravity data. Second, to acknowledge for the spatial variability of aquifer properties, we use a 2-D model for specific yield (Sy) derived from resistivity mapping and Magnetic Resonance Soundings (MRS). The latter provides a water content (θ_{MRS}) known to be higher than the specific yield. Hence, we scaled the 2-D model of θ_{MRS} with a single factor (α). WSC are calculated from water-table monitoring in the aquifer layer and neutronic measurements in the vadose layer. The value of α is obtained with a Monte–Carlo sampling approach, minimizing the RMSD between modelled and observed gravity variations. This leads to $\alpha = Sy/\theta_{MRS} = 0.63 \pm 0.15$, close to what is found in the literature on the basis of pumping tests experiments, with a RMSD value of 0.94 μGal. This hydrogeophysical experiment is a first step towards the use of time-lapse gravity data as an integrative tool to monitor interannual WSC even in complicated subsurface distribution.

Key words: Time variable gravity; Hydrogeophysics; Hydrology; Africa.

1 INTRODUCTION

Water Storage Changes (WSC) in unsaturated soils and aquifers are a key variable for water resource management, yet still challenging basement of the Sudanian zone in West–Africa, where the total storage volume is low, but shows strong annual variations (MacDonald *et al.* 2012). There, urban development relies on the ability to provide enough fresh water along the year through high yield bore-

For instance, in the surroundings of the Nikki town in the hard-rock area of northern Benin, half of the boreholes drilled in 2011 were considered as dry (Direction Générale de l'Eau, Cotonou, personal communication, 2012), despite a high mean annual rainfall of 1300 mm. Furthermore, Achidi *et al.* (2012) found a 62 per cent success rate for water drillings in crystalline basement at the country scale, against up to 90 per cent for coastal sedimentary aquifers. Seasonal WSC is thus of critical concern in this highly sensitive area, and broadening the range of methods available to monitor this key variable is a major challenge.

There are numerous approaches for the evaluation of WSC that are usually based on distributed (or not) point measurements in one or several compartments responsible for WSC [i.e. top soil, vadose zone (VZ), water tables]. For instance, Time-Domain Reflectometry (TDR) is now widespread for water content monitoring, but has several limitations such as the small sampling volume (10^{-3} m^3) of a single measurement and its limitation to the upper layers of the VZ. Deriving WSC from water-table monitoring strongly depends on the knowledge of the specific yield (Sy) parameter, and only provides WSC for the water-table fluctuation zone (WTFZ). Geophysical methods are often used to characterize underground structures for extending these point measurements. WSC at the field scale can be estimated by the interpolation of these point measurements, or by several methods such as water budget estimations or numerical modelling (Healy & Cook 2002; Scanlon *et al.* 2002). As noticed by Creutzfeldt *et al.* (2010b), Christiansen *et al.* (2011b) and several others, deriving WSC from limited point measurements is still an arduous task, despite recent developments that are often limited to the upper layers of the ground (spatial TDR measurements, high-precision lysimeters, cosmic ray neutron probes, etc.). This led some open space for the emerging hydrogravimetry method which allows to perform direct non-invasive monitoring that can be derived into integrative WSC estimations if other components affecting gravity are correctly removed (Pfeffer *et al.* 2011).

Water mass redistribution leads to variations in the Earth's gravity field, which can be measured by gravimeters. Superconducting Gravimeters (SGs) provide continuous relative gravity monitoring with very high accuracy (about 1 nm s^{-2}). Apart from very recent developments on new SGs, they are drift-prone and can hardly be moved, which are their main drawbacks for hydrological studies. For further details on SGs, see for instance Goodkind (1999) and Hinderer *et al.* (2007). Spring-based gravimeters are lower accuracy (few μGal) relative gravimeters for field prospecting. They give access to spatial gravity variations with respect to a base station, and can thus provide spatiotemporal variations with repeated measurements (Naujoks *et al.* 2008; Jacob *et al.* 2010; Pfeffer *et al.* 2013). Their lower accuracy puts them on the edge of detection for many hydrological cases for which much care must be taken to achieve the best results, leading to a second drawback, the time consumption. However, they can be a powerful tool when used together with a SG or an absolute gravimeter (AG) as a base station. AGs have the advantage to be drift-free, allowing for monitoring gravity changes at long timescales, by repeating measurements without leaving the instrument at the same place. They give direct measurements of the earth gravity field with a 10–20 nm s^{-2} (1–2 μGal) precision for the most accurate one, the FG5 model (Niebauer *et al.* 1995). The FG5 AG measures the successive positions of a free falling corner cube in a vacuum chamber, using a laser interferometer and an atomic clock. The actual gravity value along the direction of the local vertical is obtained for every drop.

Until recently, the hydrological signal has mainly been seen by the geodesy community as 'noise' to be removed from the SGs time-series—often calibrated with absolute gravity measurements—to recover small geodynamics signals. Many site-specific hydrogravimetric studies can be found in the literature (e.g. Bower & Courtier 1998; Harnisch & Harnisch 2006; Imanishi *et al.* 2006; Kroner & Jahr 2006; Van Camp *et al.* 2006; Creutzfeldt *et al.* 2008; Longuevergne *et al.* 2009; Creutzfeldt *et al.* 2010a,b; Naujoks *et al.* 2010). However, only very few studies use AGs as field instruments for measuring temporal changes due to the redistribution of water (Jacob 2009; Pfeffer *et al.* 2011). This allows to investigate other areas than single SGs observatories without being affected by the drift and accuracy limitations of the microgravimeters.

Gravity measurements are often compared to hydrological monitoring, by calculating the gravity effect of these measured WSC in a direct modelling approach (Creutzfeldt *et al.* 2008; Jacob *et al.* 2008; Creutzfeldt *et al.* 2010a; Pfeffer *et al.* 2011). A few recent studies also successfully calibrated conceptual or physical hydrological models in a coupled hydrogeophysical inversion framework such as defined by Ferré *et al.* (2009) (see also Creutzfeldt *et al.* 2010b; Christiansen *et al.* 2011a,b). However, to successfully compare gravity data and hydrological monitoring, the hydrogravimetry method is also limited by the poor spatial extent of hydrological point measurements, and by the integrative character of gravity data. The latter requires some knowledge of the WSC of each compartment in the footprint area of the gravimeter. Very few studies consider the contribution of each layer, and the VZ is usually poorly or not documented (Christiansen *et al.* 2011b). Creutzfeldt *et al.* (2010a) presented the first study which comprehensively measured WSC in all relevant storage components, namely groundwater, saprolite, soil, topsoil and snow storage, and compared them to gravity measurements.

A usual byproduct of hydrogravimetric surveys is an estimation of the specific yield (Sy) parameter, as it relates water-table fluctuations (an observation easily available) to unconfined aquifer storage variations. This can be done for various levels of precision, using relative spring-based gravimeters (Montgomery 1971; Pool & Eychaner 1995; Gehman *et al.* 2009), absolute gravity data (Jacob *et al.* 2008; Pfeffer *et al.* 2011) or even GRACE (Gravity Recovery and Climate Experiment) satellite products (Shamsudduha *et al.* 2012). However, Creutzfeldt *et al.* (2010a) pointed out that 'interpreting the regression coefficient [between gravity and water table level] in a physical way is problematic and only valid if the correlation between groundwater and other water storages can be neglected or the water mass variations in all other storages are small compared to the groundwater mass variation'. One may also add that the assertion is valid if WSC in other storages are known and their gravity effect can be calculated and removed from the regression analysis. At the field scale, Sy estimates are derived from classical hydrological experiments such as pumping tests or water budgets estimates. More recently, the emerging geophysical method of Magnetic Resonance Soundings (MRS) which determines a 'MRS water content' parameter (θ_{MRS}) was also used for estimating Sy (Healy & Cook 2002; Vouillamoz *et al.* 2005; Boucher *et al.* 2009). Comparing Sy obtained from pumping tests to θ_{MRS}, these authors observed lower Sy values with respect to θ_{MRS}, as summarized by the study of Vouillamoz *et al.* (2012) who found $Sy/\theta_{MRS} = 0.4$ for a clayey sandstones aquifer in Northern Cambodia.

In this paper, we present an AG survey carried out in a tropical weathered hard-rock unconfined aquifer context of subhumid West Africa (Nalohou, Benin: 1.6056°E–9.7424°N) during 3 yr (2009–2011) using high accuracy FG5 measurements (four measurements a year). These measurements have been carried out in the framework of the GHYRAF (Gravity and HYdRology in AFrica) project that

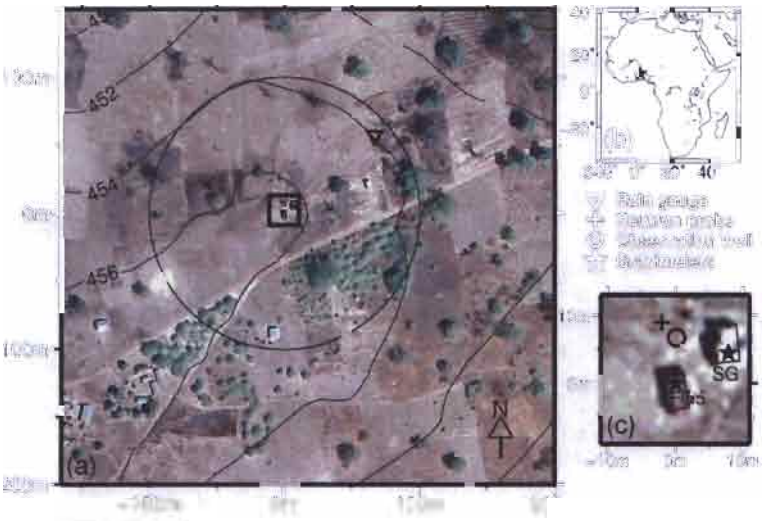
452
454
456
N
(a)
(b)
(c)
SG

of 3.48 per cent (1992–2002; Direction des études démographiques 2003). As there is almost no irrigation (rain-fed crops) so far, water consumption is mainly domestic, through the use of village wells, and is negligible in the water budget (about 0.2 mm yr^{-1}, on a basis of 20l per inhabitant per day; Séguis *et al.* 2011).

3 HYDROMETEOROLOGICAL MONITORING

Rainfall is monitored by a tipping-bucket raingauge located 100 m away from the FG5 measurement site (Fig. 1a). Cumulative and daily rainfall are shown on Fig. 2b and exhibit the seasonal rainfall pattern characteristic of the West African monsoon with wet and dry seasons. About 60 per cent of the total annual amount falls between July and September (Kamagaté *et al.* 2007). The interannual variability of rainfall is very marked in this area (e.g. Le Barbé *et al.* 2002; Le Lay & Galle 2005), and explains the divergence of these annual rainfall amounts with the mean calculated over a longer period (see section Study area), especially for 2009 and 2010 which were two particularly wet years.

Water table is measured every 2 d in a 10 m-deep OW at about 7 m of the FG5 measurement site since 2009 March (Fig. 1c). Other OWs located in the surroundings show similar variations in amplitude and phase. WSC in the WTFZ (WSC_P, $[L]$) are linked to water-table variations (Δh, $[L]$) through the specific yield Sy, using

$$WSC_P = Sy\Delta h. \quad (1)$$

Water-table time-series is shown in Fig. 2a. Maximal water-table depth occurs at the end of June/early July and is 6.3 m in average. The increase of minimum storage from 2008 to 2010 is probably linked to an early start of the rainy season and high annual rainfall in 2009 and 2010 as shown in Fig. 2(b). The late onset of the rainy season in 2011, after the wet year of 2010 is responsible for the drop in the minimum storage in 2011 June. These observations clearly show important interannual storage variations. Note that the thickness of the never-saturated VZ is about 1.7 m. From September to the following June, the groundwater depletion rate is regular and slow (12 mm d^{-1}). It has been shown that permanent groundwater does not drain into rivers through baseflow, instead groundwater depletion during the dry season (as in Fig. 2a) is more likely explained by root water uptake, even if deep drainage through fracture zones has not been discarded so far (Séguis *et al.* 2011). Another borehole located about 100 m from the gravimeter shows very similar water-table variations (less than 10 cm difference for the seasonal amplitude of about 4 m for the years 2009–2010, and much more, about 70 cm for the much drier year 2011—not presented in the study—and for which we suspect some problems). Another borehole also located about 100 m from the gravimeter, does exhibit similar water-table variations (less than 30 cm difference on the seasonal amplitude). This indicates that there are some small spatial variations of the water table, yet not directly linked to the topography or to a possible base level.

4 WATER STORAGE MONITORING

4.1 Method

About 9 m close to the OW is another 7.5-m deep borehole, but enclosed at its bottom, in which weekly measurements of soil moisture [θ,(%)] by NP are undertaken since 2009 March. For further details on NPs, the reader is referred to the IAEA training courses (IAEA 2003). Neutronic measurements are neutron counts measured in each layer of material and normalized by neutron counts acquired in the standard medium, that is, a water tank, giving counting rates (CR). Calibration is needed to transform these counting rates into

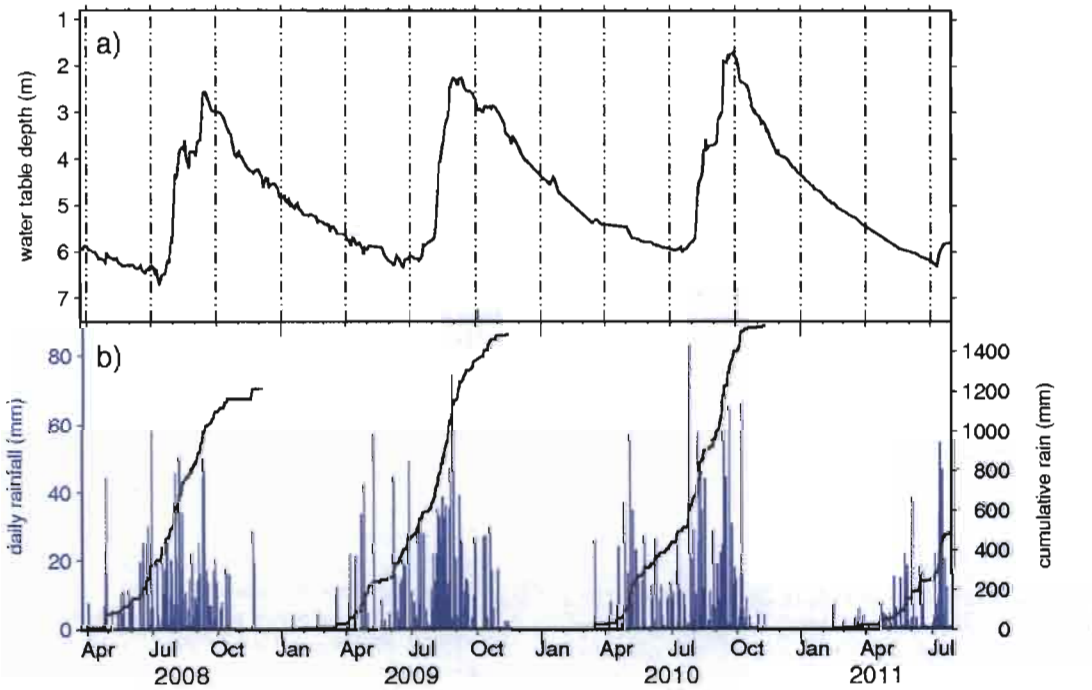

Figure 2. Hydrological data. (a) Water-table time-series. (b) Rainfall data: daily (blue) and cumulative (black). There is a gap in the rainfall data in 2011 May, but regional data show a deficit with respect to past years.

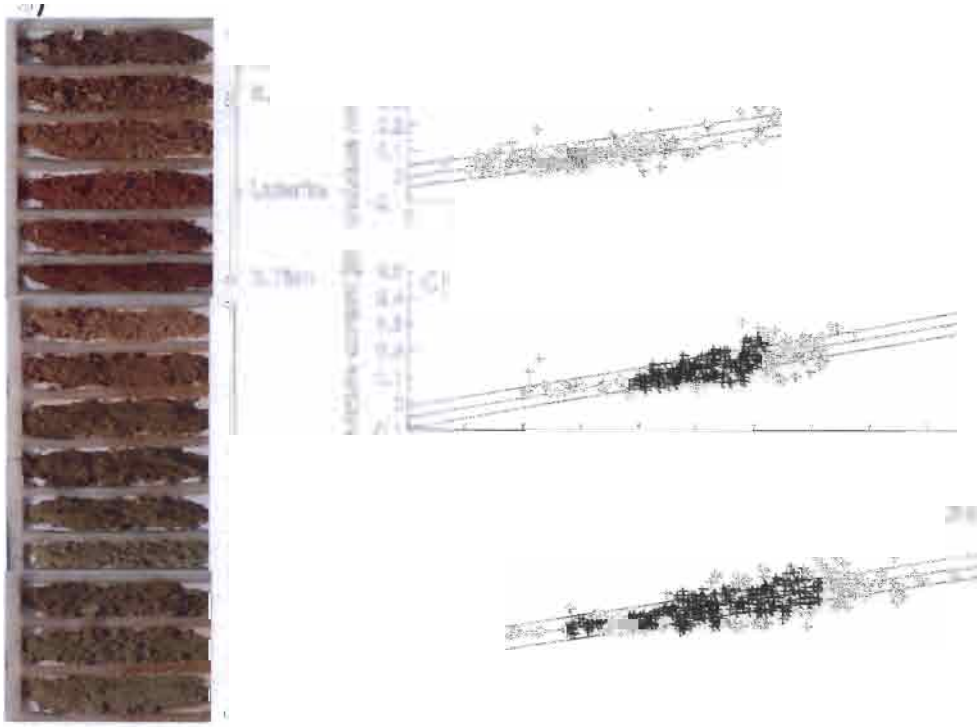

Table 1. Results of NP calibration for each class. m is the number of couples used for calibration, using the equation $\theta = a + CR \cdot b + e\sigma(CR,\theta)$ is the covariance between counting rates (CR) and moisture contents (θ), $\sigma^2()$ are variance terms for each parameter of the regression analysis and $\sigma(a,b)$ is the covariance between a and b.

Type	m	$\sigma(CR,\theta)$	b	a	σ^2(e)	$\sigma^2(b)$	$\sigma^2(a)$	$\sigma(a,b)$
Soil	142	0.0058	3.15^{E}-01	-1.20^{E}-03	1.80^{E}-03	6.76^{E}-04	7.12^{E}-05	-2.19^{E}-04
Laterite	260	0.0045	3.71^{E}-01	-5.54^{E}-02	1.40^{E}-03	4.65^{E}-04	1.24^{E}-04	-2.41^{E}-04
Alterite	373	0.0078	3.51^{E}-01	-5.83^{E}-02	2.00^{E}-03	2.36^{E}-04	7.07^{E}-05	-1.29^{E}-04

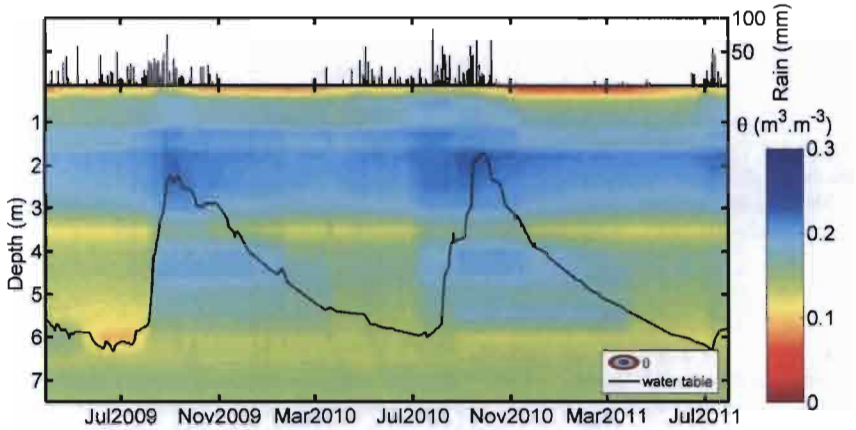

Figure 4. Time-depth evolution of water content derived from NP monitoring. Solid black line is the water-table level and daily rainfall is shown on an independent axis.

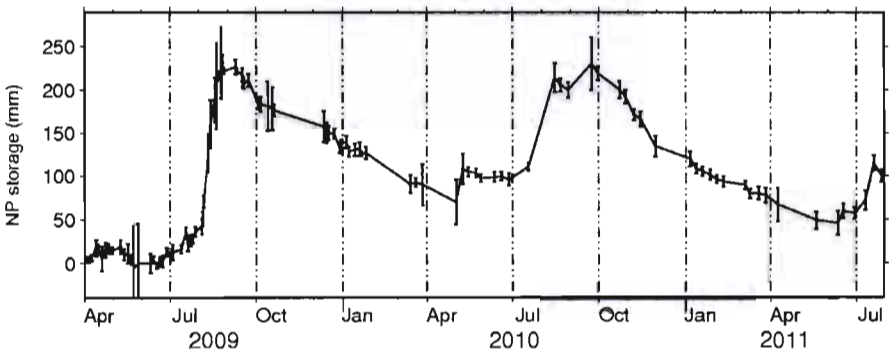

Figure 5. NP derived WSC and associated date-to-date errors.

storage in 2010 May has no obvious consequence on the water-table level). Noise in the data can be observed in the saturated zone, for which water content is supposed to remain constant. The upper part of the profile exhibits a higher water content, as can be expected from this weathered hard-rock basement context. During the dry season, storage variations in the WTFZ (i.e. below 1.7 m) are related to drainage process as evidenced by the analysis of suction data from nearby tensiometers. The two recession periods (from 2009 September to 2010 May and from 2010 September to 2011 July) produce seasonal WSC in the WTFZ of 117 and 125 mm, respectively. Once divided by the associated thickness, this gives average water content variations of 2.8 and 2.9 per cent, respectively. Because water content variations in the WTFZ during these recession periods are caused by drainage process, these val-

d t t of e t cally a 2 ag d S al e at the NP

Table 2. Mean standard deviations of WSC from NP measurements: σ(WSC), σ_I(WSC), σ_c(WSC) and σ_{int}(WSC) are mean standard deviations on respectively the derived WSC, the instrument measurement, the calibration and the integrative method used to interpolate between investigated depths (here we use the trapezoidal method).

σ(WSC)	σ_I(WSC)	σ_c(WSC)	σ_{int}(WSC)
11.6 ± 10 mm	0.16 ± 4.10^{-3} mm	0.6 ± 0.4 mm	11.6 ± 10 mm

a date-to-date storage variations basis. Standard deviation for WSC is in average 11.6 mm of equivalent water height when all possible couples of the time-series are analysed statistically, and is largely coming from the integration error (Table 2).

NP d a h e o l WSC (F 5) s w fr sr vb 150

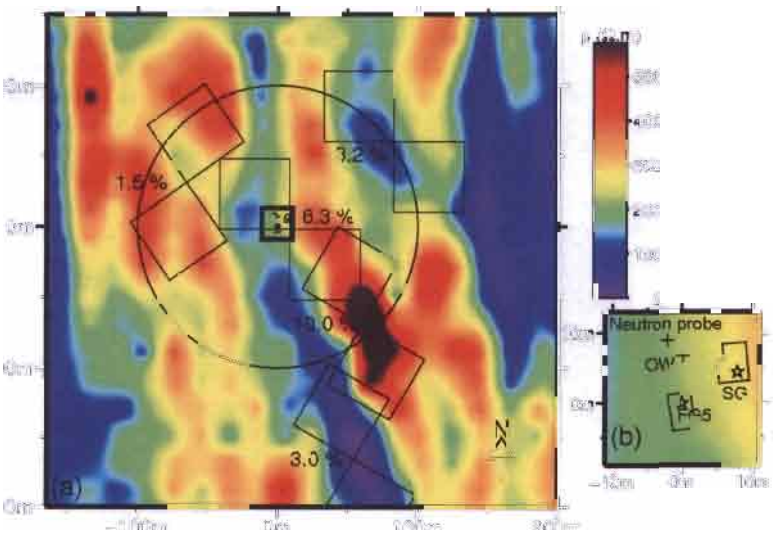
1.2 %
1.5 %
6.3 %
3.0 %
(a)
Neutron probe
OWT
SG
(b)

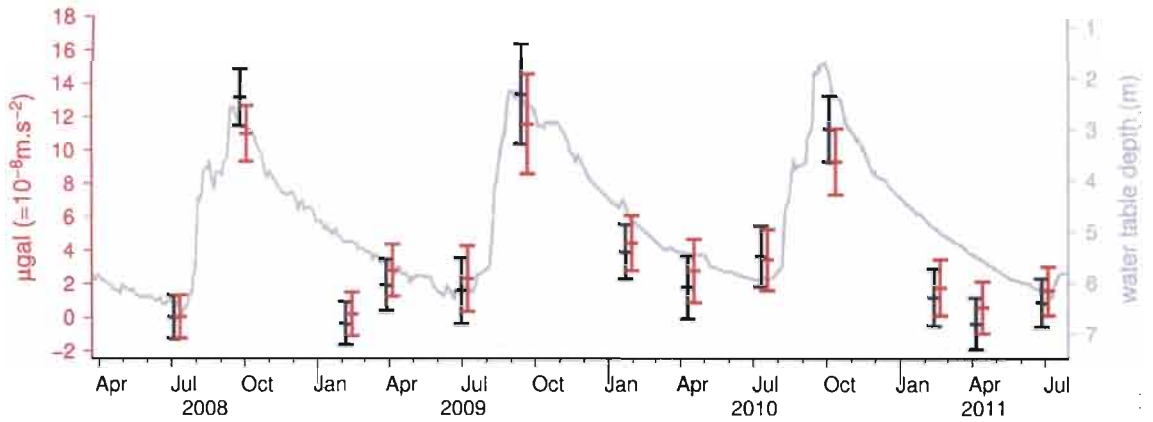

Figure 7. FG5 gravity data: raw (classical corrections applied) data in black, corrected for non-local contribution in red. Absolute values are obtained by adding 978033590.4 µGal. In background and light grey is water-table depth, plotted on an independent axe.

Nalohou. Permanently ice-covered areas (Greenland, Alaska and mountain glaciers) have been masked out and the conservation of the total water mass has been enforced by adding/removing a uniform oceanic layer compensating any lack/excess of water over land. As described in Spratt (1982) or De Linage *et al.* (2007), the Green's functions have a Newtonian term (the direct attraction of the load) and an elastic, deformation-induced term. The former is also the sum of two contributions, local and global. The local term is equal to the Bouguer analytical expression (i.e. see eq. 5 in the next section). The contribution of continental water storage within a range of a several tens of kilometres around the station is negligible if we assume a thin layer load acting on a spherical earth. In this case, the water masses are at a similar height than the gravimeter, and the vertical attraction is almost null (Llubes *et al.* 2004). We correct gravity observations for the non-local contribution, by convolving the corresponding Green's functions with the outputs of the GLDAS/Noah global hydrology model.

Gravity measurements started in 2009 July, with a rate of four measurements per year. Dates have been selected according to the hydrological cycle: at the end of June and early July, the water table is the lowest. The corrected gravity values and associated standard deviation during 3 yr from 2008 July to 2011 July are presented in Fig. 7, together with their values corrected for the non-local hydrological component. As shown by a recent study in Niger, the local and non-local hydrology contributions are in phase, the non-local one being about 20 per cent of the total effect (Pfeffer *et al.* 2011). Hence, the correction for the non-local hydrology reduces the amplitude of gravity variations of local origin. In the background of Fig. 7 is shown the water-table depth, on an independent axis. This allows to roughly compare the phase of the two signals: when groundwater recharge occurs (between July and September), there is a strong increase in gravity (around 10 µGal). One sees mainly the seasonal term since the lack of higher frequency gravity data sampling avoids finer comparisons.

7 GRAVIMETRICAL MODELING

Direct modelling of the gravitational effect of WSC ($\Delta g[LT^{-2}]$) can be achieved at first order by applying the 'Bouguer plate' model:

$$\Delta g = 2\pi\rho G H, \tag{5}$$

where ρ is the density of water $[ML^{-3}]$, G is the gravitational constant $[L^3M^{-1}T^{-2}]$ and H is the thickness of an infinite water layer $[L]$. This analytical expression can give satisfactory results in the case of a flat topography. In order to account for topographic effects, and for spatial heterogeneity of the specific yield, we use in this study a 3-D prisms model built from the prism equation provided by Leirião *et al.* (2009). The terrain has been discretized in prisms according to the topography using a local DEM (Digital Elevation Model) built from a network of points measured with differential GPS. The density of points is higher close to the gravimeter. DEM accuracy (Table 3) is derived from 1000 sets of control points randomly picked from the data set. In the region spanning 300 m around the SG, mean RMSD of DEMs with grid sizes varying from 5 to 20 m is about 0.1 m. The accuracy decreases with the spatial extent because of the lower density of points. Using this modelling approach, we simulated the effect of a 1-m thick layer of water distributed according to the topography, using 10 × 10-m^2 grid cells and obtained 44.5 µGal at the gravimeter measurement site. This

Table 3. DEM accuracy estimates. Mean and standard deviation values are calculated from 1000 sets of control points for each grid centered on the FG5 point.

Grid size (m)	Spatial extent (m)	Data points	Control points	Mean (RMSD) (m)	Std (RMSD) (m)
5	600	941	100	0.1	0.03
10	600	941	100	0.1	0.02
20	600	941	100	0.12	0.02
40	600	941	100	0.17	0.03
5	2000	2447	100	0.31	0.06
10	2000	2447	100	0.34	0.07
20	2000	2447	100	0.448	0.08

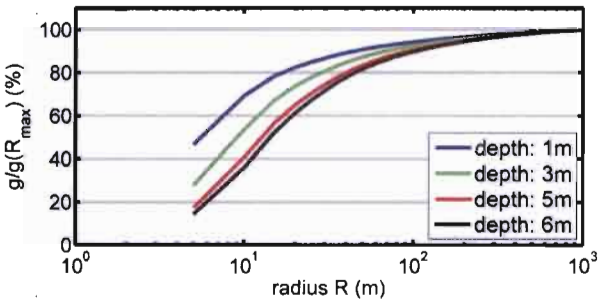

Figure 8. Ratio between the gravity effect of a 1 m layer of water in a disk centred on the FG5 with increasing radius and the gravity effect of a 1 m layer of water in a 2000-m diameter disk. Results are shown for different depths.

is slightly more than the 42 μGal derived from the Bouguer plate analytical expression, implying a small role (about 6 per cent) of the topography with respect to a flat model. The effect of the topography, in this case, results in a higher gravity variation than for the Bouguer plate. This is because the gravimeter is located on top of a hill, and more masses than in the plane geometry are located 'underneath' the gravimeter, thus increasing the vertical component affecting the gravity measure. For instance, Creutzfeldt *et al.* (2008) found a higher value of 52 μGal for SG Wettzell observatory in Germany. The gravity effect of a 1-m thick layer of water at 1, 3 and 6 m deep with respect to the topography has been calculated with different grid sizes (5, 10, 20, 30 and 40 m) from the same DGPS data set. Discrepancies in gravity never exceed 2 per cent between all different grid sizes (largest discrepancies being between the 5 m and the 40 m). This very high accuracy obtained even with coarse grids is due to the very flat terrain, with almost no high frequency variations.

The 100-m footprint area of the gravimeter, such as shown on Fig. 1a, is calculated from the ratio between the gravity effect of a 1 m layer of water in a disk centred on the FG5 with increasing radius and the gravity effect of a 1 m layer of water in a 2000-m diameter disk. This is shown on Fig. 8. 90 per cent of the signal modelled up to a radius of 1000 m come from a disk of 40 m for the 1-m deep layer of water (2.5 m below the FG5), 60 m for the 3-m deep layer of water (4.5 m below the FG5), 80 m for the 5-m deep layer of water (6.5 m below the FG5) and 85 m for the 6-m deep layer of water. The 100 m radius corresponds to 92 per cent of the signal modelled up to a radius of 1000 m for the 5-m deep layer of water, which is about the average water-table level.

This model has been applied for the two goals of the present study: (i) to compare and cross-validate NP and FG5 data; (ii) to account for spatial heterogeneity of the specific yield.

7.1 Error assessment

In the following, the relevance of the fit between observed (Δg_{FG5}) and modelled (Δg_m) gravity variation is assessed using the RMSD equation

$$\mathrm{RMSD} = \sqrt{\frac{\sum_{i=1}^{n}(\Delta g_{FG5,i} - \Delta g_{m,i})^2}{n}}, \quad (6)$$

where n is the number of available time steps.

Variances on observed absolute gravity values are obtained from the distribution of hourly set values for each experiment. Variances on gravity variations are obtained from the summation of respective variances for consecutive data points.

8 JOINT ANALYSIS OF DATA SETS: METHODS

8.1 Comparison of NP and FG5 data

Because NP measurements are made in a single borehole, a 1-D geometry is applied in the first step of this modelling approach. Water content measurements by NP in the 0–7.5 m layer are uniformly applied for each grid cell of the model, accounting for topography. Let $G[\mathrm{WSC}(t)]$ be the transformation of the storage variations through time to gravity variations. Hence,

$$\Delta g_m(\Delta t) = G\left[\mathrm{WSC}_{\mathrm{NP}(0-7.5m)}(t)\right], \quad (7)$$

where $\mathrm{WSC}_{\mathrm{NP}(0-7.5m)}(t)$ are the storage variations measured by NP through the whole vertical profile where storage variations actually occur, and Δg_m is their modelled gravity effect. The latter is compared to FG5-derived gravity variations, and relevance of the fit is evaluated with the RMSD (eq. 6).

The instrument is protected by a 12 m^2 shelter. This modifies the local infiltration in the vicinity of the instrument ('mask effect'), and consequently the lack of close infiltration has been evaluated. This mask effect is taken into account by considering two extreme cases, (i) no soil moisture variations underneath the shelter, or (ii) they are exactly the same as without shelter. The first case is obtained by subtracting to the total modelled signal the gravity effect from WSC occurring underneath the shelter.

One should keep in mind that FG5 measurements are spatially integrated, while NP produces point-measurements. The 1-D assumption made here can be inappropriate because 2-D structures have been evidenced with surface geophysics.

Error assessment

The confidence interval on modelled gravity variations is simply calculated as the gravity effect of the NP-derived storage time-series; with $\pm 1\sigma$ uncertainty in NP values (as shown on Fig. 5, calculated using eq. 3).

8.2 2-D model for specific yield

The water-table fluctuations can be considered as representative over the 100 m radius around the FG5 site, as confirmed by the similarity exhibited by different water-table measurements carried out close to the site. Considering water-table fluctuations in the saturated zone of the model allows hence to account for spatial variability of the storage through Sy mapping. For unconfined aquifers, mass variations in the saturated zone are directly linked to the specific yield. Its value and spatial distribution control the amount of water that produces gravity variations (Pool & Eychaner 1995). A 2-D model for θ_{MRS} is shown in Fig. 9. Cells size is 20 × 20 m^2 large in the vicinity of the gravimeter and 50 × 50 m^2 further away. Taking smaller cells had no influence, because of the relatively flat topography (see Section 7). Also, the resolution of resistivity mapping is not precise enough to describe a possible structure for θ_{MRS} at finer scales.

Numerous studies showed that θ_{MRS} is somewhat different from Sy (Vouillamoz *et al.* 2005; Boucher *et al.* 2009; Vouillamoz *et al.* 2012) and rather close to the effective porosity, defined as the portion

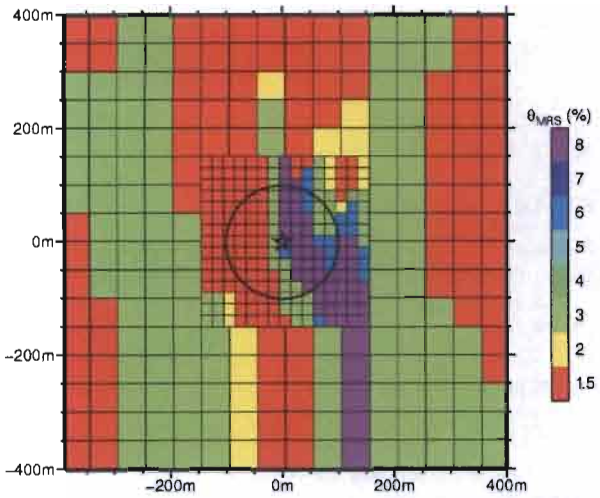

Figure 9. 2-D model for θ_{MRS} obtained through the spatialization of MRS water contents using resistivity mapping and geological observations. The circle shows the 100-m radius zone of influence for the FG5 gravimeter.

of a medium that contributes to the flow and advective transport (Lubczynski & Roy 2005). Knowing this, we scaled the 2-D model by a factor α, using

$$Sy = \alpha\theta_{MRS}(x, y), \tag{8}$$

where $\theta_{MRS}(x, y)$ stands for the spatial distribution of the MRS water content.

Gravity variations from the WTFZ and the VZ are modelled by

$$\Delta g_m(\Delta t) = G\left[\Delta h \alpha \theta_{MRS}(x, y) + \mathrm{WSC}_{NP(VZ)}(t)\right], \tag{9}$$

where Δh is the water-table variations uniformly distributed according to the topography. It is then possible to optimize the α parameter (eq. 9) with respect to FG5 data, minimizing the RMSD (eq. 6).

It is also possible to derive a 1-D equivalent Sy parameter, by adjusting a single value of Sy over the whole area without taking into account the spatial variability. To derive a 1-D equivalent Sy value is highly interesting for hydrological models, or for any further attempt to use gravity data as a proxy for water storage monitoring.

8.3 Error assessment

Variances on modelled gravity variations are estimated for the two contributing compartments (WTFZ and VZ). For the WTFZ, water-table measurements can be considered to be quite accurate. If we hypothesize an uncertainty of 1 cm on the reading, with an average Sy value of 5 per cent, this leads to a 0.5 mm error on storage estimation, which is insignificant compared to NP measurements errors (as shown on Table 2). However, spatial variations of the water table in the vicinity of the gravimeter site are not taken into account in this study. As specified in Section 3, other boreholes exhibit similar variations, and discrepancies seem not to be correlated to spatial variations of θ_{MRS}, as one could expect a correlation between water-table levels and Sy. For the VZ (the 0–1.7 m layer), standard deviations on NP-derived storage variations are obtained using eq. 3. Then, their gravity effect has been calculated using the present model.

To get the best-fitting α value, a simple Monte–Carlo approach is adopted: 40 000 sets of (modeled VZ gravity contribution, observed FG5 data) scattered couples are randomly sampled within their distribution in both dimensions, assuming they are normally distributed. These distributions are defined by their mean values and standard deviations based on the error assessments of observed gravity variations and modelled VZ contributions. For each set, the contribution of the WTFZ is added by testing a range of α values. The best-fitting α for each set is found by minimizing the RMSD (eq. 6). We eventually obtain both the mean value and standard deviation of the resulting α distribution.

9 JOINT ANALYSIS OF DATA SETS: RESULTS

9.1 1-D model: cross-validation of NP and FG5 data

The first result of this study arises from the comparison of gravity data with direct water content measurements by NP in the 0–7.5 m layer (the whole profile where WSC occur), from which the gravity effect is calculated using the aforementioned model (Fig. 10). In this figure, as we are dealing with storage variations, each modelled time-series is vertically shifted with an offset that minimizes the distances to FG5 data points. When considering the mask effect of the shelter (i.e. no WSC underneath the shelter), the

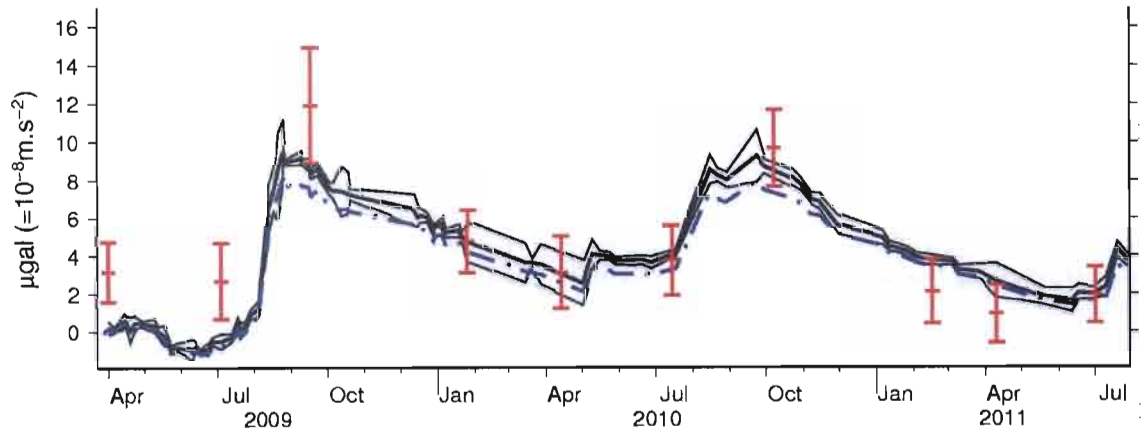

Figure 10. FG5 data (red points with error bars) and gravity modelling of NP-derived storage variations (black line). Light black curves show the confidence interval at $\pm 1\sigma$. Dashed blue curve takes into account the mask effect of the shelter (i.e. no WSC underneath the shelter).

calculation produces a time-series that remains most of the time within the error bars of the former (blue curve in Fig. 10). The comparison shows a fair agreement when considering respective error bars (RMSD = 1.61 μGal). Discrepancies between gravity measurements and the water storage model made out of point measurements can be related to the non-representativeness of the NP data (point measurements in a specific borehole) with respect to the larger zone 'seen' by the gravimeter. This is particularly true in case of strong local heterogeneities. Hence, the next step is to introduce the spatial distribution of θ_{MRS}, known to be close to Sy.

9.2 2-D model and specific yield estimation

Fig. 11 shows the results of the 2-D model for specific yield (black curve), derived from MRS and resistivity mapping, assuming that $\theta_{MRS} = Sy$ (i.e. $\alpha = 1$). The gravity data, within their standard deviation, are not so well adjusted to the modelled water storage variations, particularly for the 'wet' point in 2010 and the two points in 2009 April and July. The black curve comes from the summation of two contributions, the VZ and the WTFZ. Relative contributions from the VZ and the WTFZ are 20 and 80 per cent, respectively, enlightening that now 80 per cent of the model does account for spatial heterogeneities of the specific yield. Furthermore, the underlying assumption of spatial homogeneity in the upper (VZ) layer needs to be valid in a smaller area (see Fig. 8). The RMSD of the fit is 2.5 μGal, and associated scatter plot is shown on Fig. 12(a) (black points). Recent data from six other NP boreholes located within the 100 m radius of influence of the gravimeter indicated a mean seasonal amplitude in the VZ of 74 ± 10 mm for the 2011–2012 hydrological year. This standard deviation of 10 mm of equivalent water thickness corresponds to 0.44 μGal when using the linear relationship of 0.044 μGal mm^{-1} (see Section 7). This is small compared to the seasonal signal, and to the RMSD of the fit, assuming little impact of using a single borehole for the VZ.

The WTFZ can produce the same contribution if we consider a uniform model of $\theta_{MRS\_equi-D} = 0.07$. This value is retrieved by assuming an homogeneous layer with a constant specific yield value in the WTFZ, and testing a range of values until the same curve as the one coming from the spatial model $\theta_{MRS}(x, y)$ with $\alpha = 1$ (Fig. 11) is qualitatively found (i.e. results with = 1 are exactly the same as when using a uniform layer with $Sy = 0.07$). This value can be seen as an averaged θ_{MRS} within the footprint area of the gravimeter, somehow weighted by an inverse square distance function.

When using the 2-D model (eq. 9), it is thus possible to find the optimal α value, with respect to gravity data, by minimizing the RMSD (eq. 6). Results are shown on Fig. 11 (blue line) for the time-series, and on Fig. 12(a) (blue points) for the fit between

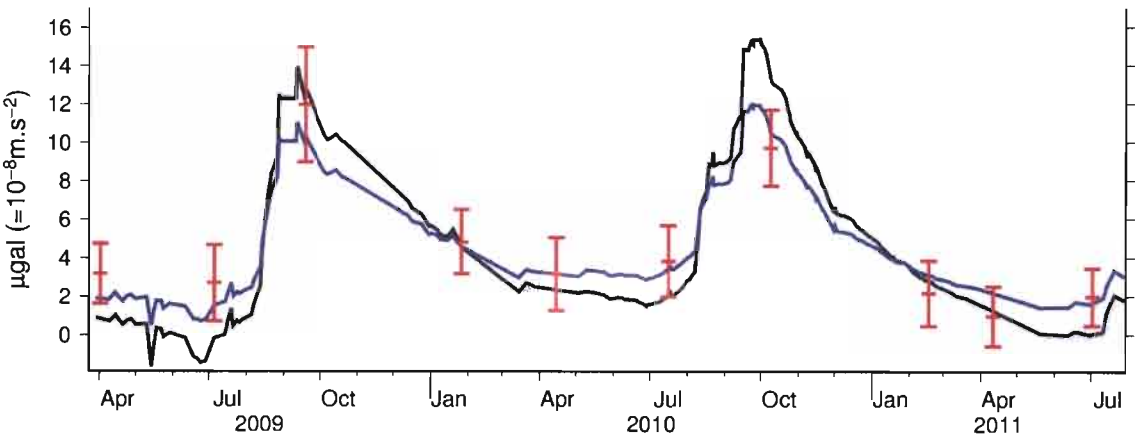

Figure 11. FG5 data (red points with error bars) and gravity modelling of hydrological effect: black and blue curves are the sum of the VZ contribution and the WTFZ contribution with respectively the spatialized θ_{MRS}, with $\alpha = 1$ (black), or with the best-fitting α value (blue).

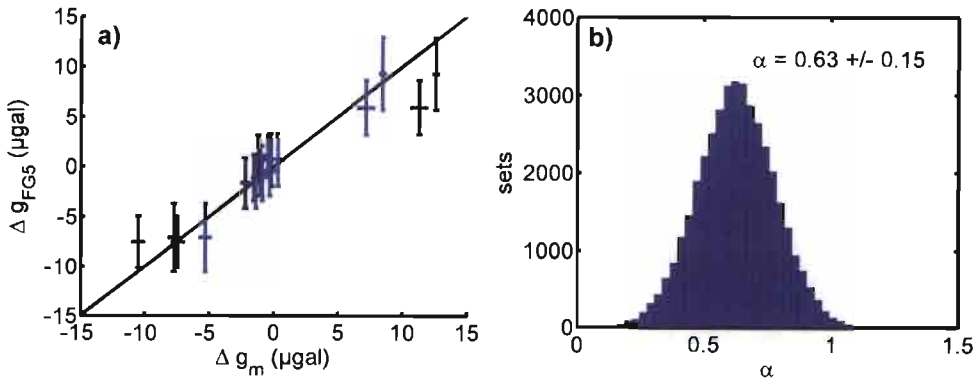

Figure 12. (a) Scatter plot of gravity variations (model and data) for both the distributed model $\theta_{MRS}(x, y)$ with $\alpha = 1$ (black points) and the best-fitting α value (blue points) and respective error bars. (b) Distribution of optimized α values for the 40 000 sets of (modelled VZ gravity contribution, observed FG5 data) scattered couples.

Model	1-D NF	2-D $\theta_{MRS}(x, y)/\alpha = 0$	2-D $\alpha = 2.85 \pm 0.15$
RMS$_G$ (μGal)	1.61	2.50	0.94
Correlation coefficie	`97	0	
.' Value	2 ×		
1-D equivalen Sy (per cent)		7	

insights for hydrologists by providing new kind of integrated observations, as long as non-hydrological components can effectively be corrected from the signal.

11 CONCLUSION

In this study, absolute gravity data from FG5 monitoring have been compared to modelled gravity variations derived from WSC measurements by NP and water-table level. Gravity data have been corrected for solid earth tides, ocean loading, air pressure effects, polar motion contribution and non-local hydrology and residuals are associated to local WSC and show seasonal variations of up to 11 μGal. This is somewhat higher than gravity variations deduced from NP only and distributed according to the topography, using a 0.1-m accuracy DEM. NP data have the advantage to investigate the whole profile where WSC occur in this weathered hard-rock basement context. Drawbacks of comparing NP data to gravity data are the local character of the former, with respect to the integrated nature of the second.

Spatial heterogeneities of the WTFZ were taken into account in the second part of this study, by scaling a factor of a 2-D model for θ_{MRS} on the basis of gravity residuals. This resulted in a significant decrease of the RMSD between gravity residuals and the modelled signal and thus militates for the proper modelling of the spatial distribution of WSC, especially in such heterogeneous medium.

ACKNOWLEDGEMENTS

This work has been performed within the frames of the ANR GHYRAF project and the AMMA-CATCH observation system. The authors would like to thank numerous people who helped to achieve this work. Calvo M., Bernard J.D., and Tahirou Sarè for FG5 measurements, Imorou I., Pagou E., Ouani T., Afouda S., for hydrological acquisition, and Ferhat G. for topographic mapping. We would also like to thank the project partners who allowed the use of their infrastructure and provided valuable information and advices. From the Direction Générale de l'eau (DG-Eau, Cotonou): Gbodogbé J.C. and Zannou A., from the Abomey-Calavi university: Yalo N. Creutzfeldt B. and another anonymous reviewer deserve a special mention for the very complete and constructive review that significantly helped to improve the present paper.

REFERENCES

Achidi, J.B., Bourguet, L., Elsaesser, R., Legier, A., Paulvé, E. & Tribouillard, N., 2012. *Carte hydrogéologique du Bénin,* 1:500 000, Ministère de l'Energie, des recherches pétrolières et minières, de l'eau et du développement des énergies renouvelables.

AMMA database, 2013. Available at: http://database.amma-international.org. (last accessed 3 April 2013).

Le Barbé, L., Lebel, T. & Tapsoba, D., 2002. Rainfall Variability in West Africa during the Years 1950–90., *J. Clim.,* **15,** 187–202.

Boucher, M., Favreau, G., Vouillamoz, J.M., Nazoumou, Y. & Legchenko, A., 2009. Estimating specific yield and transmissivity with magnetic resonance sounding in an unconfined sandstone aquifer (Niger), *Hydrogeol. J.,* **17,** 1805–1815.

Bower, D. & Courtier, N., 1998. Precipitation effects on gravity measurements at the Canadian Absolute Gravity Site, *Phys. Earth planet. Int.,* **106**(3–4), 353–369.

Boy, J.-P., 2012. GGP loading. Available at: http://loading.u-strasbg.fr/GGP/10.1093/gji/ggt146.html. Accessed 1 April 2013.

Boy, J.-P. & Hinderer, J., 2006. Study of the seasonal gravity signal in superconducting gravimeter data, *J. Geodyn.,* **41**(1–3), 227–233.

Christiansen, L., Binning, P., Rosbjerg, D., Andersen, O.B. & Bauer-Gottwein, P., 2011a. Using time-lapse gravity for groundwater model calibration: an application to alluvial aquifer storage, *Water Resour. Res,* **47,** doi:10.1029/2010WR009859.

Christiansen, L., Haarder, E.B., Hansen, A.B., Looms, M.C., Binning, P., Rosbjerg, D., Andersen, O.B. & Bauer-Gottwein, P., 2011b. Calibrating vadose zone models with time-lapse gravity data, *Vadose Zone J.,* **10,** 1–11.

Creutzfeldt, B., Guntner, A., Klugel, T. & Wziontek, H., 2008. Simulating the influence of water storage changes on the superconducting gravimeter of the Geodetic Observatory Wettzell, Germany, *Geophysics,* **73**(6), WA95–WA104, doi:10.1190/1.2992508.

Creutzfeldt, B., Güntner, A., Thoss, H., Merz, B. & Wziontek, H., 2010a. Measuring the effect of local water storage changes on in situ gravity observations: case study of the Geodetic Observatory Wettzell, Germany, *Water Resour. Res,* **46,** W08531, doi:10.1029/2009WR008359.

Creutzfeldt, B., Güntner, A., Vorogushyn, S. & Merz, B., 2010b. The benefits of gravimeter observations for modelling water storage changes at the field scale, *Hydrol. Earth Sys. Sci.,* **14**(9), 1715–1730.

Descloitres, M., Séguis, L., Legchenko, A., Wubda, M., Guyot, A. & Cohard, J.M., 2011. The contribution of MRS and resistivity methods to the interpretation of actual evapo-transpiration measurements: a case study in metamorphic context in north Bénin, *Near Surface Geophys.,* **9**(2), 187–200.

Direction des études démographiques, 2003. *Recensement de la Population 2003,* Institut National de la Statistique et de l'Analyse Économique, Benin.

Dubus, N. & Dubus, J., 2011. *La sécheresse au Sahel: Vers une gestion concertée,* Hermes Science Publications, Paris.

Farrell, W.E., 1972. Deformation of the Earth by surface loads, *Rev. Geophys.,* **10**(3), 761–797.

Ferré, T. *et al.*, 2009. Critical steps for the continuing advancement of hydrogeophysics, *EOS, Trans. Am. Geophys. Un.,* **90**(23), 200, doi:10.1029/2009EO230004.

Gehman, C.L., Harry, D.L., Sanford, W.E., Stednick, J.D. & Beckman, N.A., 2009. Estimating specific yield and storage change in an unconfined aquifer using temporal gravity surveys, *Water Resour. Res.,* **45,** W00D21, doi:10.1029/2007WR006096.

Goodkind, J.M., 1999. The superconducting gravimeter, *Rev. Sci. Instrum.,* **70**(11), 4131–4152.

Guyot, A., Cohard, J.-M., Anquetin, S., Galle, S. & Lloyd, C.R., 2009. Combined analysis of energy and water balances to estimate latent heat flux of a sudanian small catchment, *J. Hydrol.,* **375**(1–2), 227–240.

Harnisch, G. & Harnisch, M., 2006. Hydrological influences in long gravimetric data series, *J. Geodyn.,* **41**(1–3), 276–287.

Healy, R.W. & Cook, P.G., 2002. Using groundwater levels to estimate recharge, *Hydrogeol. J.,* **10**(1), 91–109.

Healy, R.W. & Scanlon, B.R., 2010. *Estimating Groundwater Recharge,* Cambridge University Press, Cambridge.

Hinderer, J., Crossley, D. & Warburton, R.J., 2007. 3.04—gravimetric methods—superconducting gravity meters, in *Treatise on Geophysics,* pp. 65–122, ed. Schubert, G., Elsevier, Amsterdam.

Hinderer, J. *et al.*, 2009. The GHYRAF (Gravity and Hydrology in Africa) experiment: description and first results, *J. Geodyn.,* **48**(3–5), 172–181.

Hinderer, J. *et al.*, 2012. Land water storage changes from ground and space geodesy: first results from the GHYRAF (gravity and hydrology in Africa) experiment, *Pure Appl. Geophys.,* **169**(8), 1391–1410.

IAEA, 2003. *Neutron and Gamma Probes: Their Use in Agronomy,* IAEA.

Imanishi, Y., Kokubo, K. & Tatehata, H., 2006. Effect of underground water on gravity observation at Matsushiro, Japan, *J. Geodyn.,* **41**(1–3), 221–226.

Jacob, T., 2009. Apport de la gravimétrie et de l'inclinométrie à l'hydrologie karstique, *PhD thesis,* Université de Montpellier II.

Jacob, T. *et al.*, 2008. Absolute gravity monitoring of water storage variation in a karst aquifer on the larzac plateau (Southern France), *J. Hydrol.,* **359**(1–2), 105–117.

... heterogeneity of a karst aquifer, ...
... doi:10.1029/2009JB006...
..., Seidel, J.-L., Descloitres, M. ...
... hydriques d'un bassin versant ... Donga, haut Ouémé), Compte ...
...
... determination of the surface resistivi...
... 741–757.
... experiments around the superco... J. Geodyn., 41(1–3), 268–27...
... Variabilités interannuelle et intra-saisonnière ... en contexte ouest-africain ...

... Global Geodynamics Project and ... case studies, J. Geodyn., 38, 355– ...

... N., Viville, D., Ferhat, G., Ulrich, ... local and global hydrological contributions ... Strasbourg, J. Geodyn., 40(3–5), 189– ...

... MRS contribution to hydrogeological ... Surface Geophys., 5(3), 121–135.
... Dochartaigh, B. & Taylor, R.G., 2012. ... resources in Africa, Environ. Res. Lett., ...
... ation of coefficient of storage by use ... Department of Geosciences, University of ...

... Jahr, T., Kroner, F. & Hinnen, S., 2010. ... modelling by temporal gravity observations ... model, Geophys. J. Int., 182(1), 223– ...

Am. Meteorol. Soc., 88, 381–394.
Scanlon, B., Healy, R. & Cook, P., 2002. Choosing appropriate techniques for quantifying groundwater recharge, Hydrogeol. J., 10(1), ...
Schwiderski, E.W., 1980. Ocean tides, part I: a global ocean tidal equation model, Mar. Geod., 3(1–4), 161–...
Séguis, L. et al., 2011. Origins of streamflow in a crystalline basement catchment in a sub-humid Sudanian zone: the Donga basin (Benin, West Africa): inter-annual variability of water budget, J. Hydrol., 402(1–2), 1–13.
Shamsudduha, M., Taylor, R.G. & Longuevergne, L., 2012. Monitoring groundwater storage changes in the highly seasonal humid tropics: validation of GRACE measurements in the Bengal Basin, Water Resour. Res., 48(2), doi:10.1029/2011WR010993.
Spratt, R.S., 1982. Modelling the effect of atmospheric pressure variations on gravity, Geophys. J. R. astr. Soc., ...
Van Camp, M., Vanclooster, M., Crommen, O., Petermans, T., Verbeeck, K., Meurers, B., Van Dam, T. & Dassargues, A., 2006. Hydrogeological investigations at the Membach station, Belgium, and application to correct long periodic gravity variations, J. geophys. Res., 111, B10403, doi:10.1029/2006JB004405.
Vandervaere, J.P., Vauclin, M., Haverkamp, R. & ... 1998. ... analysis in estimating soil water ... the HAPEX-Sahel experiment ... J. Hydrol., ... 370.
Vouillamoz, J.M., Descloitres, M., Toe, G. & Legchenko, A., 2005. Characterization of crystalline basement aquifers with MRS: comparison with boreholes and pumping tests data in Burkina Faso, Near Surface Geophys., 3(3), 205–213.
Vouillamoz, J.M., Sokheng, S., Bruyere, O., Caron, D. & Arnout, L., 2012. Towards a better estimate of storage properties of aquifer with magnetic resonance sounding, J. Hydrol., 458–459, 51–58.
Wenzel, H., 1996. The nanogal software: Earth tide data processing package ETERNA 3.30, Bull. d'Inform. des Marées Terrestres, 124, 9425–9439.